PAPER

Check for updates

Surface characteristics of thin film composite polyamide membranes dictate silver nanoparticle loading efficacy†

Afsana Munni,[abc] Mohammed A. Bashammakh,[ab] Marion Bellier,[ab] Ali Ansari, [iD][ac]
Mohamed E. A. Ali, [iD][abd] H. Enis Karahan, [iD][abe] Rafiqul Islam,[c]
Treavor H. Boyer[a] and François Perreault [iD] *[abf]

Silver nanoparticles (AgNPs) have emerged as promising antimicrobial agents for controlling biofilm growth on polyamide (PA) thin film composite membranes. However, the current literature lacks a clear path for leveraging silver functionalization in designing biofouling-resistant PA membranes mainly due to huge variations in the resulting silver loading on the membrane. To help develop a robust procedure for fabricating AgNP-loaded PA membranes, here we investigate the relationship between loading yield and membrane (surface) properties. We selected four commercially available PA TFC membranes (BW 30, SW 30 XLE, AMI H, NF 270) and decorated those with AgNPs using the same functionalization chemistry. As expected, we observed a clear variation in silver loading (in the order of BW 30 > AMI H > SW 30 > NF 270). To elucidate the role of membrane surface properties in determining the silver loading efficacy, we conducted a detailed surface characterization of PA TFC membranes using atomic force microscopy, X-ray photoelectron spectroscopy, Fourier-transform infrared spectroscopy, streaming potential analysis, and contact angle measurements. Subsequently, we employed multiple linear regression analysis to correlate surface properties with silver loading. Our investigation revealed that oxygen content significantly influences AgNP loading ($p < 0.05$), more than any other surface characteristics. These results will guide future material selection for reverse osmosis or nanofiltration applications critical in the water sector in short term. Moreover, the insights gained from this work are expected to be pivotal in developing membranes more suitable for fabricating AgNP-loaded antimicrobial membranes.

1. Introduction

Membrane-based water/wastewater treatment and seawater desalination processes are arguably among the most promising ways for addressing the growing water scarcity,[1] making the role of thin film composite (TFC) membranes used in reverse osmosis (RO) and nanofiltration (NF) applications even more crucial.[2] The cutting-edge RO and NF membranes are

developed by creating relatively thin crosslinked polyamide (PA) coatings on support layers, which enable efficient contaminant removal and salt rejection under conditions exceeding the osmotic pressure of feed solutions.[3] The membrane selection is made according to the specific treatment goals; while the NF membranes are used for the removal of hardness-causing impurities and organic matter,[4,5] the RO membranes serve for almost complete demineralization at high energy efficiency.[4–6] The differences in crosslinking density and monomer selection for interfacial polymerization (of the PA layer) control the selectivity and permeability of resulting TFC membranes and their suitability for NF/RO processes.

The polymerization conditions of the selective PA layer greatly influence the surface characteristics of the resulting membranes in terms of both chemical and morphological aspects. During the interfacial polymerization (IP) process, a difunctional amine (dissolved in water) and a trifunctional acid chloride (dissolved in a water immiscible organic phase) are reacted. Commonly used amines

[a] School of Sustainable Engineering and the Built Environment, Arizona State University, Tempe, AZ 85287, USA. E-mail: perreault.francois@uqam.ca

[b] Nanosystems Engineering Research Center for Nanotechnology-Enabled Water Treatment, Arizona State University, Tempe, AZ 85287, USA

[c] Cactus Materials Inc., Tempe, AZ 85282, USA

[d] Egypt Desalination Research Center of Excellence (EDRC) & Hydrogeochemistry Department, Desert Research Center, Cairo, 11753, Egypt

[e] CNRS, Immunology, Immunopathology and Therapeutic Chemistry, UPR 3572, 67000 Strasbourg, France

[f] Department of Chemistry, University of Quebec in Montreal, CP 8888, Succ. Centre-Ville, Montreal, QC, H3C 3P8, Canada

† Electronic supplementary information (ESI) available. See DOI: https://doi.org/10.1039/d4lf00088a

include m-phenylenediamine (MPD) in RO membranes and piperazine (PIP) in NF membranes, while trimesoyl chloride (TMC) is the acid chloride of choice for both cases.[2] The fast reaction kinetic results in the formation of three-dimensionally crosslinked coating at the interface of the porous support and liquid reaction mixture, presenting residual amine (–NH_2) and carboxylic (–COOH) functionalities at the surface.[3] The carboxyl groups form through the hydrolysis of acid chloride groups during and after the IP process while the amine groups, usually in smaller quantities, originate from the unreacted end groups of the aminated monomers.[2] This difference in surface chemistry and morphology resulting from the IP conditions determines the membranes' long-term effectiveness, by defining key factors like surface charge and roughness.[2,7]

The fouling phenomena, especially biofouling, pose major challenges for PA TFC membranes.[8,9] Microorganisms are commonly found in any water treatment scenarios, and their surface attachment to membranes can lead to biofilm formations.[9,10] Notably, membrane (bio)fouling results in an increase in energy consumption for water treatment and a decrease in the membrane lifetime due to the increased frequency of chemical treatments required for surface cleaning. To control microbial growth and biofilm formation, disinfectants such as chlorine are commonly employed in wastewater treatment; however, such oxidants can degrade the selective PA layers.[11,12] To address these challenges and control biofilm formation without using oxidants, researchers have turned to nanomaterials to modify membrane surfaces and introduce new functionalities[4,8] The materials used for antibiofouling surface functionalization can be broadly divided into materials that impart anti-adhesive properties, like superhydrophilic silica NPs[13,14] or materials that impart antimicrobial properties, like metallic NPs, carbon nanomaterials, or photocatalytic NPs.[15–17] Among antimicrobial materials, which have a critical role in the control of microbial growth once they reach the membrane, materials predominantly functioning through contact-based mechanisms like graphene oxide or carbon nanotubes have the advantage of not dissolving over time, which helps retain the antimicrobial performance of the membrane surface.[18,19] However, contact-based materials lose their activity once covered by a layer of cellular material (*e.g.*, dead cells), which gives them limited functionality over time. Alternatively, nanomaterials that release toxic compounds to inactivate bacteria in the vicinity of the membrane have been widely used on PA TFC membranes due to their high efficiency and ease of functionalization; however, these antimicrobial NPs often act by slowly releasing toxic elements into the water, which leads to their eventual depletion and the need to regenerate the coating. Common metal and metal oxide systems used for antimicrobial properties include silver, copper, selenium, and bismuth oxide nanoparticles.[20–23]

Among the different antimicrobial nanomaterials used, silver is one of the most popular because of its high antimicrobial efficacy against bacteria, viruses and other eukaryotic micro-organisms, their low toxicity to humans, and their simple nucleation chemistries.[15,24,25] Silver nanoparticles (AgNPs) endow antimicrobial activity to membrane surfaces by enabling silver ion (Ag^+) release and expanding the surface area for microbial inactivation. Several studies have established that AgNPs of 10–100 nm in size show strong biocidal properties in water treatment systems, enhancing membrane performance by mitigating fouling[11,26,27] and improving flux.[28] In the case of PA TFC membranes, AgNPs can be integrated to the PA surfaces through two main approaches, *i.e.*, *in situ* nucleation of AgNPs on the surface and *ex situ* synthesis of AgNPs, which are then integrated into the monomer solutions during interfacial polymerization.[23,29–31] Each method has its own advantages and limitations. For example, the *ex situ* synthesis provides more opportunities to control the size and surface chemistry of the AgNPs that are to be integrated into the PA layer; however, such coatings cannot be regenerated once the AgNPs are depleted during operation. On the other hand, membranes have been shown to be able to be re-coated several times by the *in situ* technique.[32] Being a post-fabrication functionalization, it is also easy to integrate to the membrane fabrication system or even to apply to pre-made commercially available membrane modules.[23,28,31,33] Therefore, among these surface functionalization techniques, *in situ* reduction of Ag^+ ions (to zerovalent AgNPs) is highly popular with its practicality and applicability to commercially available systems.[23,26,27,29]

Different types of PA membranes have been functionalized by *in situ* growth of AgNPs, yielding varying degrees of silver loadings (summarized in Table S1†). For example, Yang *et al.*[34] used polydopamine (PDA) to nucleate AgNPs on a RO membrane (XLE), achieving a loading of 0.2 to 13.3 μg cm^{-2} and a significant reduction in viable bacteria for *Escherichia coli* (*E. coli*) and *Bacillus subtilis*.[34] Ben-Sasson *et al.*[23] developed an antimicrobial RO membrane by nucleating AgNPs on SW 30 membranes using varying ratios of AgNO_3 : NaBH_4, which resulted in a silver loading range of 0.82 to 3.7 μg cm^{-2} and high inactivation of *E. coli*. Similarly, Wu *et al.* used NaBH_4 to nucleate AgNPs on NF membranes modified with different treatments, which resulted in various silver loadings (from 1.85 to 3.75 μg cm^{-2}) and high bacterial inactivation.[35] Soroush *et al.* achieved 80% bacterial inactivation with a silver loading of nearly 4 μg cm^{-2} on a forward osmosis PA TFC membrane using AgNPs nucleated on a graphene oxide support.[36] These studies collectively demonstrate the broad interest in using AgNPs to impart antimicrobial properties to water treatment membranes.[11,26,37] However, since these studies were done using a range of nucleation chemistries, it is hard to decouple the impact of the PA properties and particle growth chemistry.

The main objective of this research was to identify the key surface properties that influence the loading of AgNPs in PA membranes. To achieve this, four different types of commercial RO and NF membranes (SW 30, BW 30, AMI H, and NF 270) were thoroughly characterized before being coated with AgNPs using the same nucleation chemistry. The resulting AgNP-loaded membranes were then characterized using elemental analysis and electron microscopy. This systematic approach enabled us to pinpoint the most influential property affecting silver loading on the membrane surface through multiple linear regression (MLR) analysis. Our findings offer deeper insights into AgNP functionalization of PA TFC membranes and provide guidelines for selecting the most optimal membrane characteristics for fabricating antimicrobial membranes.

2. Materials and methods

2.1. Materials and reagents

All the chemicals and supplies used in the experiments were of ACS grade or higher and were acquired from Sigma-Aldrich (Saint Louis, MO). The membranes used in the study were BW 30, SW 30 XLE, and NF 270 from DuPont (FilmTec™) and AMI H from Hydranautics. These membranes are all PA TFC membranes but designed for different applications, namely seawater desalination (SW30), brackish water desalination (BW 30), residential tap water desalination (AMI H), and hardness and organic compound removal (NF 270). Unless mentioned otherwise, all the solutions were prepared using deionized (DI) water obtained from the GenPure UV xCAD plus ultrapure water purification system by Thermo Scientific (Waltham, MA).

2.2. Membrane modification by *in situ* formation of AgNPs

For membrane modification, the protocol reported by Ben-Sasson *et al.*[23] was followed. Briefly, the dry PA TFC membranes were wetted in a mixture of 20% isopropanol and 80% DI water for a duration of 20 min and then rinsed three times with DI water. The unfunctionalized and washed membranes were used as control samples. The *in situ* formation of AgNPs on the membrane was performed as follows: the membrane was positioned with the selective layer facing up between a glass plate and a plastic frame (with a window size of 7.5 cm × 12 cm) to hold the modifying solutions. Initially, 50 mL of a 3 mM $AgNO_3$ solution was poured on the PA layer agitated for 10 min. Then, the $AgNO_3$ solution was removed, leaving a thin layer of absorbed solution on the surface. Subsequently, 50 mL of 3 mM $NaBH_4$ solution was added and agitated for 5 min to create AgNPs on the membrane surface. Afterward, the solution was discarded, and the membrane was rinsed with 20 mL of DI water for 10 s to remove excess reagents. All the reactions were performed at room temperature.

2.3. Membrane characterization

The membrane wettability was assessed using contact angle (CA) measurements on an Attention Theta Instrument (Biolin Scientific, Paramus, NJ), employing a 1001 TPLT Hamilton syringe from Reno, NV. Six different areas were measured per membrane, and each measurement involved the recording of ∼200 data points over 10 s, which were then averaged and reported as the final mean, displayed as average ± standard deviation. The surface charge was measured *via* streaming potential measurement on a ZetaCAD analyzer equipped with a flat surface cell (CAD instruments, Les Essartes-le-Roi, France). A stable opening during testing was ensured with a 0.1 mm spacer. An electrolyte solution containing 5 mM KCl and 0.1 mM $KHCO_3$ was used for the analysis, and measurements were conducted at a pH of 8 (to represent the functionalization condition) with a pressure range of 30–70 psi. Four replicate measurements were performed for each membrane. The elemental surface composition of the membrane was examined using X-ray photoelectron spectroscopy (XPS) on a Kratos Axis Supra+ equipped with mono-Al K-alpha X-ray sources and a hemispherical analyzer combined with a spherical mirror analyzer. The measurements were performed using built-in ESCApe software, and data analyses were conducted using CasaXPS software (version 2.3.18). Fourier-transform infrared spectroscopy (FT-IR) was performed on a Bruker IFS 55 V/S FT-IR system which included a diamond attenuated total reflectance module. The membrane morphology was examined on a scanning electron microscopy (SEM) setup using an Aurica Focused Ion Beam SEM system (Zeiss, Germany) coupled with an energy dispersive X-Ray fluorescence (EDX) detector operated under an accelerating voltage of 10 kV. The specimens were gold-sputter coated before SEM analyses. The surface roughness measurements were taken on a Bruker MM8 HR instrument equipped with a conductive atomic force microscopy (AFM) head, a *J*-type tube scanner, and a Nanoscope V controller. Nunano scout 350RAI cantilevers were employed, and the sample mounting was done using double-sided tape on 15 mm magnetic specimen discs (Ted Pella). The Milty Zerostat 3 was used to treat the area of interest between measurement locations to minimize static build-up effects and measurements taken at three different spots for each sample were displayed as the mean roughness (Ra) ± standard deviation using the Bruker Nanoscope software analysis.

2.4. Silver loading quantification

The silver loading of the modified AgNP membranes was determined by inductively coupled plasma-mass spectroscopy (ICP-MS, Thermo Scientific iCap Qtega ISDS). Circular membrane coupons, having a surface area of 1.27 cm^2, were subjected to acid digestion using 10% trace metal grade HNO_3 and agitated for one day to dissolve silver from the membranes. Subsequently, the concentration of dissolved silver was quantified using ICP-MS. This analysis was

conducted in duplicate for each of three points on every membrane.

### 2.5. Data analysis and statistics

All tests were performed on at least three independent replicates to assess the variability of membrane properties. Mean values and standard deviations were calculated for each property. Multiple linear regression (MLR) analysis was performed in Excel to establish the relationship between silver loading and membrane properties. This analysis included regression statistics, where the adjusted R-squared value indicates the percentage of independent variables accounted for in the model. Furthermore, ANOVA, coefficient, standard errors, t-statistics, and p-value were used to assess the significance of these findings ($p < 0.05$).

3. Results and discussion

3.1. Functionalization of PA TFC membranes with AgNPs

The membrane selection aimed to cover a range of commonly used RO and NF membranes, representing applications from seawater RO desalination (SW 30) to brackish water RO (BW 30), tap water RO (AMI H), and NF (NF 270). In Fig. 1, the inset photos display the pristine membranes before and after functionalization. *In situ* reduction of silver ions was used to create AgNPs on the TFC RO/NF membranes.[23] This method involves introducing a diluted silver nitrate ($AgNO_3$) solution to the selective layer, leading to the interaction of silver ions (Ag^+) with negatively charged carboxylic acid groups.[38] This interaction may favor the formation of AgNPs during the reduction process.[23] Following the removal of the $AgNO_3$ solution, a residual film covers the selective layer, and subsequently, the reducing agent (sodium borohydride, $NaBH_4$) acts on the free Ag^+ in the residual film to form zerovalent AgNPs on the membrane according to eqn (1)[39–41] as described by Song *et al.*[42] The incorporation of AgNPs provides a distinctive yellow color to the membranes (Fig. 1).

$$Ag^+ + BH_4^- + 3H_2O \rightarrow Ag^0 + B(OH)_3 + 3.5H_2 \tag{1}$$
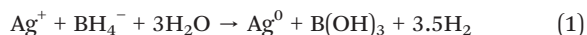
A noticeable difference in surface morphologies is observed between RO and NF membranes before and after AgNPs coating when analyzed by SEM imaging. All pristine membranes show a top surface that exhibits the typical "ridge and valley" feature of PA layers[43] in SEM images
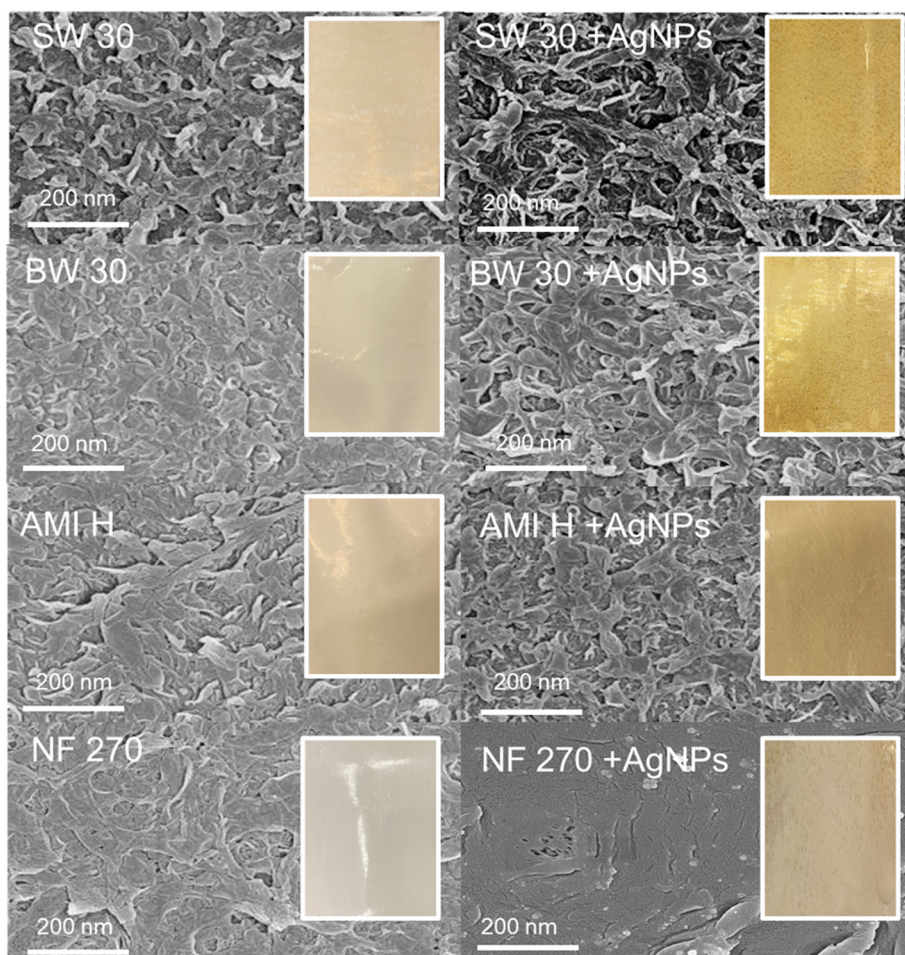

Fig. 1 SEM imaging and digital photos (insert) of the pristine and AgNP-functionalized membranes.
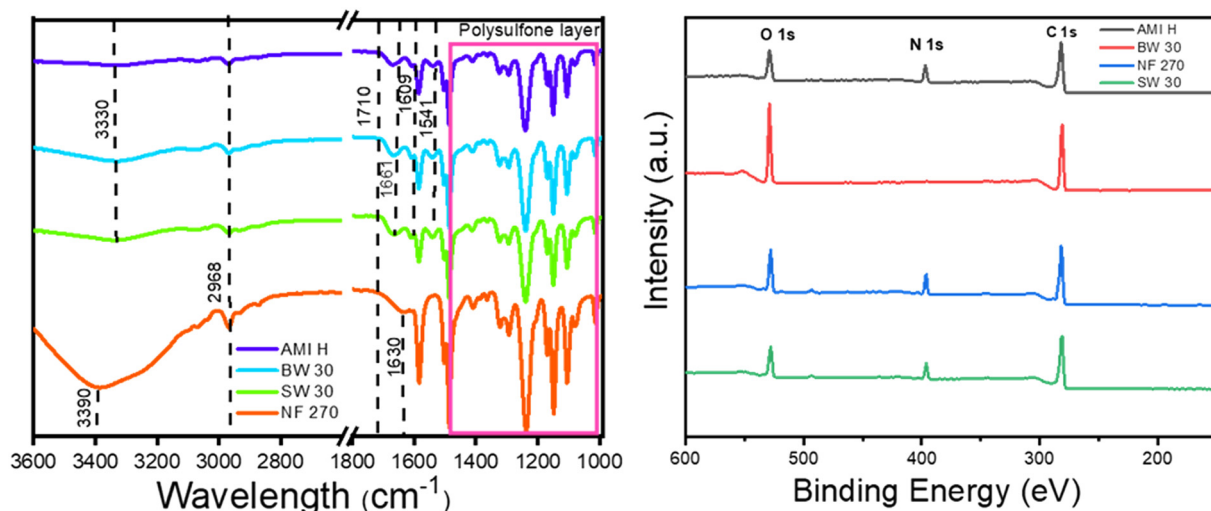
Fig. 3 FT-IR spectra (left) and XPS survey scans (right) of the different pristine membranes used for AgNP functionalization.

2968 cm^{-1}. Collectively, the presence and characteristics of these peaks strongly support that NF 270 is categorized as a semi-aromatic membrane.[7,48,53]

To gain deeper insights on the nature of surface chemistry, XPS analyses were used. XPS has a typical probing depth of around 3–5 nm and is therefore a highly sensitive method to characterize the surface chemistry of the PA layer.[47] The XPS spectra, normalized to the carbon (C 1s) peak at 284.6 eV, are presented in (Fig. 3B) for each membrane type. The PA layer is shown to be mainly composed of oxygen (O), nitrogen (N), and carbon (C). The elemental composition is detailed in Table 1, with the RO and NF membranes shown to contain approximately 70.2–77.7% C, 2.0–11.0% N, and 12.7–25.3% O. While the elemental composition was similar among the tested membranes, the BW 30 membrane is distinct in the fact that it has the lowest N ratio (3.4 ± 1.4) and the highest O ratio (23.9 ± 1.5). In pure PA, the O/N ratio reflects the degree of crosslinking with a theoretical O/N ratio of 1:1 for fully crosslinked PA (crosslinking degree is practically 100%) and 2:1 for the linear PA layer (crosslinking degree is 0%).[2,7] The ratio of O/N for BW 30 is notably higher (8.2 ± 3.5) than these theoretical values (Table 1), which suggests the presence of another layer on the PA surface that provides high oxygen content to the BW 30 membrane. This high O/N ratio could

indicate for example the presence of a hydrophilic coating, which is typically used on PA TFC membranes to increase the fouling resistance of desalination membranes. Our findings are consistent with previous studies where a high O/N ratio was also noted for BW 30 membranes.[7,48] Being on the surface of the membrane, this coating layer will also interact with the silver nucleation process during membrane functionalization.

The high-resolution XPS spectra for C 1s are displayed in Fig. 4. For each membrane, peak fittings were normalized with respect to the C–C component (284.6 eV) to estimate the binding energy (δ_{BE}) and chemical structure. A positive δ_{BE} indicated (Table S2†) that the elements are bonded to electron-withdrawing atoms such as O, Cl, and F.[2,48] All the membranes exhibit a major peak at 284.6 eV, which can be assigned to C–C/C–H bonds (aliphatic/aromatic) and a minor peak at 287.4 eV, assigned to O=C–O or O=C–N groups (carboxylic/amide groups). Furthermore, there is an intermediate peak at 286.0 eV associated with weakly electron withdrawing elements, such as carbon in C–O bonds.[2,48] These intermediate peaks indicate the possible presence of a coating or a modification during the IP reaction, observed in all RO and NF membranes. Notably, BW 30 and NF 270 membranes exhibit a higher percentage of C–O bonds

Table 1 Elemental composition, O to N ratio (O/N), membrane properties (roughness, contact angle, and streaming potential), and AgNP loading yield for the commercial TFC RO and NF membranes

Sample label	XPS-based surface element analysis				Membrane properties			AgNP loading yield[a] (%)
	O%	N%	C%	O/N	Roughness (Ra)	Contact angle	Streaming potential (at pH 8)	
SW 30	13.1 ± 0.4	9.9 ± 1.1	77.1 ± 0.6	1.3 ± 0.2	44.2 ± 2.5	54.9 ± 1.3	-33.7 ± 1.2	10.1 ± 1.7
BW 30	23.9 ± 1.4	3.4 ± 1.4	72.7 ± 1.9	8.2 ± 3.5	46.4 ± 2.4	51.3 ± 2.1	-28.0 ± 0.5	14.7 ± 0.5
AMI H	13.9 ± 0.3	9.2 ± 0.7	77.0 ± 0.7	1.5 ± 0.13	39.1 ± 1.7	68.1 ± 0.3	-42.3 ± 0.9	10.5 ± 1.0
NF 270	15.1 ± 0.4	9.6 ± 0.2	75.3 ± 0.4	1.6 ± 0.06	27.6 ± 1.2	30.4 ± 3.1	-64.1 ± 4.2	8.4 ± 0.5

[a] AgNP loading yields were calculated by the actual loading on the basis of ICP-MS results divided by the initial concentration of the silver used for membrane coating.
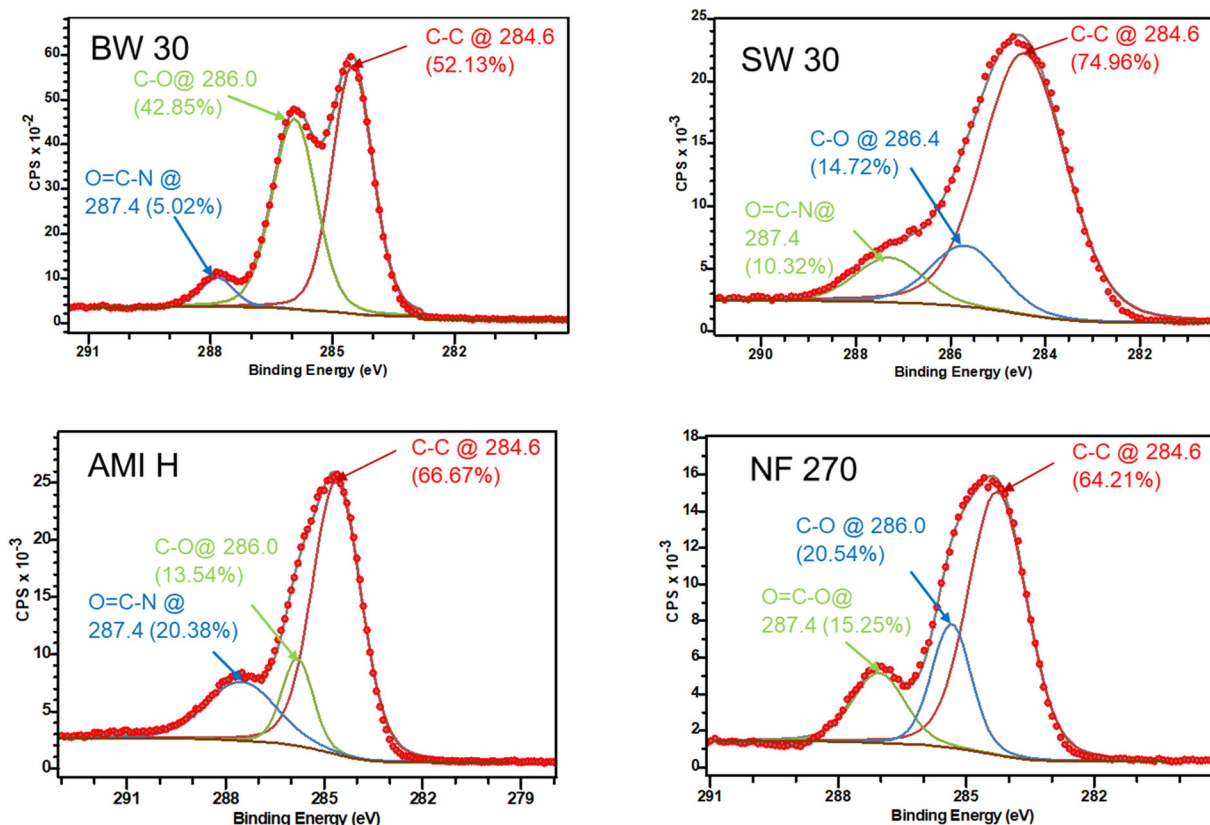
Fig. 4 High-resolution XPS spectra (C 1s) of TFC RO and NF pristine membranes.

(Fig. 4), implying a greater level of coating or modification compared to AMI H and SW 30 membranes. This observation aligns with the FT-IR observations in the range of 3700–2700 cm^{-1}. Additionally, NF 270 exhibits a C–O bond percentage of ~20.5%, which is about half of the C–O bond percentage in the BW 30 membrane, at 42.9% (Fig. 4). Altogether, the XPS analysis shows notable differences in surface chemistry among the different membranes, which likely influences the silver functionalization (AgNP loading) process.

3.3. Surface charge and wettability

The changes in surface chemistry described above will influence the surface charge and wettability that is, in part, determined by the nature of the functional groups on the surface. For example, deprotonation of –COOH to –COO$^-$ contributes to the negative surface charge of PA membranes at pH values above the pK_a of carboxylic acids. Different pK_a values are reported in the literature for different types of PA TFC membranes, with typically two pK_a for carboxylic functional groups at ~3 and 5 (ref. 54 and 55) which means that these groups will be mostly negatively charged at the pH condition used for silver functionalization. The surface charges of different membranes were characterized using streaming potential measurement and it was found that all the membranes were negatively charged (at pH 8). The range of zeta potential values of the different membranes was

between −20 and −65 mV (Table 1). Interestingly, the fully aromatic PA layer of brackish water (BW 30 and AMI H) and sea water (SW 30) membranes showed a less negative zeta potential than the semi-aromatic PA layer of NF 270. A more negative charge may provide more binding sites that create a favorable environment for stable AgNP adsorption.[2,44,56] However, when compared to the AgNP loading results of Fig. 2, this effect does not appear to be important for the silver functionalization used in this work.

Besides the functional groups on the surface of the membranes, silver loading can also be influenced by the roughness and wettability of the PA surface.[46,49] Membrane roughness represents irregularities at the surface, which was quantified by AFM topographical imaging using the average roughness (Ra) parameter, which is associated with the height deviation from mean surface levels[46] Fig. S2† and 5 present two-and three-dimensional images where light and dark areas correspond to peaks and valley structure, respectively. Furthermore, Fig. 5 shows the crumpled structure commonly observed in RO and NF membranes for all pristine membranes. The roughness analyses of all the RO membranes show similar values (Table 1). Notably, the NF 270 membrane exhibited lower roughness (Ra of 27.6 ± 1.2 nm), which is attributed to the stable interface formed during the IP reaction between TMC and PIP, known to result in typically smoother PA layers.[50] The smoother NF 270 surface is explained by its looser configuration of the PA polymer in
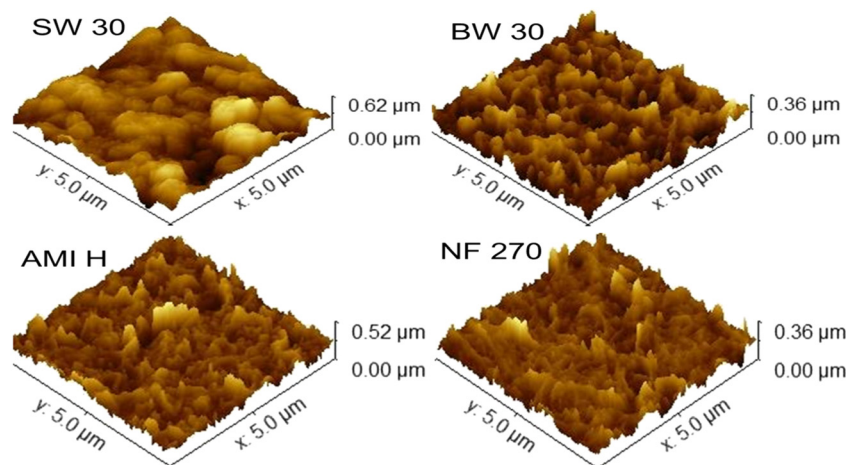

Fig. 5 Three-dimensional images of surface roughness of all pristine membranes.

contrast to the tightly structured fully aromatic PA layer of RO membranes.[50] The increase in surface roughness follows the order of BW 30 > SW 30 > AMI H > and NF 270. A similar trend is found for silver loading, which suggests that the greater availability of sorption sites provided by the rougher surface may be a factor in determining the silver loading on PA TFC membranes.

Finally, surface wettability, which is influenced by both surface chemistry and roughness, is also a factor that can influence the resulting silver loading during AgNP nucleation. Among others, surface wettability can affect the heterogeneous particle nucleation rate on the surface.[57] Fully aromatic and semi-aromatic membranes exhibit different contact angles. BW 30, SW 30, and AMI H membranes have contact angles within a range of (30–70°), while that of NF 270 falls significantly lower (25–35°) than RO membranes. Previous studies have indicated that membranes with high hydrophilicity, characterized by an abundance of carboxylic or hydroxylic groups, offer more reaction sites for the attachment of silver on the surfaces.[2,44,56] However, in this study, BW 30 displayed the highest silver loading while having lower hydrophilicity compared to NF 270 (Table 1). Moreover, the silver loading for AMI H and SW 30 was not significantly different, despite SW 30 having a lower contact angle than AMI H (Table 1). Therefore, the contact angle seems to be an unreliable predictor of silver loading, especially considering variations in contact angle values found in the literature for commercial membranes, which complicate direct dataset comparison.[2,50,58]

3.4. Statistical validation of surface-loading correlation

Based on the characterization results shown above, several factors clearly influence the silver loading efficacy. For example, despite a general trend of lower silver loading with smoother PA surfaces, SW 30 and BW 30 have similar surface roughness values but showed different silver loadings.

Similarly, SW 30 and AMI H have almost the same O/N ratio but displayed different silver loadings, despite the potential role of $-COO^-$ groups in adsorption of Ag^+ ions on PA membranes. Hence, to establish a correlation between membrane properties and silver loading, a multiple linear regression (MLR) analysis was performed to identify the most important parameters for AgNP functionalization of PA TFC membranes.

When silver loading on the different PA TFC membranes is correlated with surface roughness (Ra parameter from AFM analysis), wettability (water contact angle), surface charge (streaming potential at pH 8), and oxygen content (% O, from XPS analyses), the MLR model ($R^2 = 0.84$) reveals that the most influential property for silver loading is the oxygen content. The overall F-test of the MLR model resulted in a p value of 0.000256, indicating a high degree of confidence that at least one of the surface properties has an influence on the silver loading after AgNP functionalization.[59] Analysis of the coefficient table presented in Table 2 shows that all variables had a p value above 0.05 except for the oxygen content, which showed a high degree of confidence ($p = 0.0050$) and the highest coefficient value (94.77), which both support its high influence on the resulting silver loading after AgNP functionalization (Table 2). Overall, the statistical analysis indicates that oxygen content is the most influential property across all the membranes. Notably, in this study, BW 30 exhibits a significantly higher O content (Table 1) compared to

Table 2 MLR analysis of the relationship between silver loading on functionalized membranes and the surface properties of the pristine commercial membranes. Each variable category had 4 data points, for a total of 16 observations

	Coefficients	t-Stat	p-Value
Intercept	830.2	0.2881	0.7786
Roughness	27.46	0.6896	0.5047
Oxygen%	94.77	3.493	0.0050
Zeta potential (at pH 8)	10.26	0.4185	0.6836
Contact angle	1.112	0.1060	0.9174

© 2024 The Author(s). Published by the Royal Society of Chemistry

RSC Appl. Interfaces, 2024, **1**, 1186–1197 | **1193**

Paper

to the other membranes, which resulted in this membrane also having the highest silver loading.

4. Conclusion and implications for surface functionalization processes

The objective of this study was to identify the most important membrane properties that influence the AgNP loading efficacy of the widely employed *in situ* particle growth approach. The oxygen content stands out as the most critical factor for increased Ag loading on PA TFC membranes. The oxygen content may be provided by the chemical nature of the PA layer. Alternatively, as in the BW 30 case, the application of an oxygen-rich surface coating could be leveraged to increase the AgNP loading efficacy. These findings have practical implications for developing AgNP-functionalized antibiofouling membranes for advanced water treatment applications.

The functionalization chemistry used in this study was selected to mimic the typical roll-to-roll production processes used for membrane fabrication. In this fabrication scenario, the membrane would be in contact with one solution at a time, first the Ag^+ solution and then the reducing agent. The nucleation of AgNPs on the PA TFC membrane may represent the first step in the functionalization process. For example, it is known that pristine AgNPs dissolve over time, which would result in a loss of biocidal activity. A subsequent step therefore could be the passivation of the AgNPs with sulfides or halides, which has been shown to slow down the dissolution process and extend the lifetime of the silver coating.[39,60] The silver-coated surfaces can also be further modified with anti-adhesive functionalities using polymeric materials such as zwitterionic brushes, providing dual benefits of reducing bacterial adhesion as well as slowing down silver release.[61] For all these surface functionalization processes, nucleation of the AgNPs on the surface will be the initial step. Therefore, understanding the surface properties that will dictate the silver loading efficiency is of broad importance for silver-based antimicrobial coatings.

In addition, the identification of the surface properties relevant for silver loading can find broader use for other types of materials, such as nylon,[62] textiles,[63] or paper[45] that have been functionalized with AgNPs for biocidal applications. Therefore, future work should aim to extend the framework developed in this study to a broader range of surface chemistries, compared using similar functionalization conditions, in order to provide more general coating efficiency predictors for the functionalization of various materials with AgNPs.

Conflicts of interest

There are no conflicts of interest.

Acknowledgements

References

1 G. Vaseghi, A. Ghassemi and J. Loya, Characterization of reverse osmosis and nanofiltration membranes: effects of operating conditions and specific ion rejection, *Desalin. Water Treat.*, 2016, **57**(50), 23461–23472, DOI: **10.1080/19443994.2015.1135825**.

2 C. Y. Tang, Y. N. Kwon and J. O. Leckie, Effect of membrane chemistry and coating layer on physiochemical properties of thin film composite polyamide RO and NF membranes II. Membrane physiochemical properties and their dependence on polyamide and coating layers, *Desalination*, 2009, **242**, 168–182, DOI: **10.1016/j.desal.2008.04.004**.

3 D. M. Stevens, J. Y. Shu, M. Reichert and A. Roy, Next-Generation Nanoporous Materials: Progress and Prospects for Reverse Osmosis and Nanofiltration, *Ind. Eng. Chem. Res.*, 2017, **56**(38), 10526–10551, DOI: **10.1021/acs.iecr.7b02411**.

4 D. L. Zhao, S. Japip, Y. Zhang, M. Weber, C. Maletzko and T. S. Chung, Emerging thin-film nanocomposite (TFN) membranes for reverse osmosis: A review, *Water Res.*, 2020, **173**(15), 115557, DOI: **10.1016/j.watres.2020.115557**.

5 N. García Doménech, F. Purcell-Milton and Gun'ko YK., Recent progress and future prospects in development of advanced materials for nanofiltration, *Mater. Today Commun.*, 2020, **23**, 100888, DOI: **10.1016/j.mtcomm.2019.100888**.

6 R. R. Choudhury, J. M. Gohil, S. Mohanty and S. K. Nayak, Antifouling, fouling release and antimicrobial materials for surface modification of reverse osmosis and nanofiltration membranes, *J. Mater. Chem. A*, 2018, **6**(2), 313–333, DOI: **10.1039/c7ta08627j**.

7 C. Y. Tang, Y. N. Kwon and J. O. Leckie, Effect of membrane chemistry and coating layer on physiochemical properties of thin film composite polyamide RO and NF membranes: I. FTIR and XPS characterization of polyamide and coating layer chemistry, *Desalination*, 2009, **242**, 149–167, DOI: **10.1016/j.desal.2008.04.003**.

8 L. Tang, K. J. T. Livi and K. L. Chen, Polysulfone membranes modified with bioinspired polydopamine and silver

nanoparticles formed in situ to mitigate biofouling, *Environ. Sci. Technol. Lett.*, 2015, **2**(3), 59–65, DOI: **10.1021/acs.estlett.5b00008**.

9   W. Ma, A. Soroush, T. Van Anh Luong, G. Brennan, M. S. Rahaman, B. Asadishad and N. Tufenkji, Spray- and spin-assisted layer-by-layer assembly of copper nanoparticles on thin-film composite reverse osmosis membrane for biofouling mitigation, *Water Res.*, 2016, **99**, 188–199, DOI: **10.1016/j.watres.2016.04.042**.

10 B. Mi and M. Elimelech, Organic fouling of forward osmosis membranes: Fouling reversibility and cleaning without chemical reagents, *J. Membr. Sci.*, 2010, **348**(1–2), 337–345, DOI: **10.1016/j.memsci.2009.11.021**.

11 Y. Zhang, Y. Wan, Y. Shi, G. Pan, H. Yan, J. Xu, M. Guo, L. Qin and Y. Liu, Facile modification of thin-film composite nanofiltration membrane with silver nanoparticles for anti-biofouling, *J. Polym. Res.*, 2016, **23**, 105, DOI: **10.1007/s10965-016-0992-7**.

12 J. Yin and B. Deng, Polymer-matrix nanocomposite membranes for water treatment, *J. Membr. Sci.*, 2015, **479**, 256–275, DOI: **10.1016/j.memsci.2014.11.019**.

13 B. Díez, N. Roldán, A. Martín, A. Sotto, J. A. Perdigon-Melon, J. Arsuaga and R. Rosal, Fouling and biofouling resistance of metal-doped mesostructured silica/polyethersulfone ultrafiltration membranes, *J. Membr. Sci.*, 2017, **526**, 252–263, DOI: **10.1016/J.MEMSCI.2016.12.051**.

14 A. Tiraferri, Y. Kang, E. P. Giannelis and M. Elimelech, Superhydrophilic thin-film composite forward osmosis membranes for organic fouling control: Fouling behavior and antifouling mechanisms, *Environ. Sci. Technol.*, 2012, **46**(20), 11135–11144, DOI: **10.1021/ES3028617/SUPPL_FILE/ES3028617_SI_001.PDF**.

15 B. Fadeel and A. E. Garcia-Bennett, Better safe than sorry: Understanding the toxicological properties of inorganic nanoparticles manufactured for biomedical applications, *Adv. Drug Delivery Rev.*, 2010, **62**(3), 362–374, DOI: **10.1016/J.ADDR.2009.11.008**.

16 L. Azeez, A. Lateef and O. Olabode, An overview of biogenic metallic nanoparticles for water treatment and purification: the state of the art, *Water Sci. Technol.*, 2023, **88**(4), 851–873, DOI: **10.2166/WST.2023.255**.

17 B. A. Omran and M. Abdel-Salam, Chapter 16 - A new age of innovative technology for wastewater treatment using nanomaterials, *Microbial Ecology of Wastewater Treatment Plants*, 2021, 331–358, DOI: **10.1016/B978-0-12-822503-5.00011-4**.

18 A. Tiraferri, C. D. Vecitis and M. Elimelech, Covalent binding of single-walled carbon nanotubes to polyamide membranes for antimicrobial surface properties, *ACS Appl. Mater. Interfaces*, 2011, **3**(8), 2869–2877, DOI: **10.1021/AM200536P/SUPPL_FILE/AM200536P_SI_001.PDF**.

19 F. Perreault, M. E. Tousley and M. Elimelech, Thin-Film Composite Polyamide Membranes Functionalized with Biocidal Graphene Oxide Nanosheets, *Environ. Sci. Technol. Lett.*, 2014, **1**(1), 71–76, DOI: **10.1021/ez4001356**.

20 X. Xu, H. Zhang, T. Gao, J. Teng and M. Lu, Antibacterial thin film nanocomposite forward osmosis membranes produced by *in situ* reduction of selenium nanoparticles, *Process Saf. Environ. Prot.*, 2021, **153**, 403–412, DOI: **10.1016/J.PSEP.2021.07.037**.

21 M. Khorram, F. Nabizadeh Chianeh and M. Shamsodin, Preparation and characterization of a novel polyethersulfone nanofiltration membrane modified with Bi2O3 nanoparticles for enhanced separation performance and antifouling properties, *J. Ind. Eng. Chem.*, 2022, **114**, 456–474, DOI: **10.1016/J.JIEC.2022.07.036**.

22 M. Ben-Sasson, K. R. Zodrow, Q. Genggeng, Y. Kang, E. P. Giannelis and M. Elimelech, Surface functionalization of thin-film composite membranes with copper nanoparticles for antimicrobial surface properties, *Environ. Sci. Technol.*, 2014, **48**(1), 384–393, DOI: **10.1021/ES404232S/SUPPL_FILE/ES404232S_SI_001.PDF**.

23 M. Ben-Sasson, X. Lu, E. Bar-Zeev, K. R. Zodrow, S. Nejati, G. Qi, E. P. Giannelis and M. Elimelech, In situ formation of silver nanoparticles on thin-film composite reverse osmosis membranes for biofouling mitigation, *Water Res.*, 2014, **62**, 260–270, DOI: **10.1016/j.watres.2014.05.049**.

24 M. Rai, A. Yadav and A. Gade, Silver nanoparticles as a new generation of antimicrobials, *Biotechnol. Adv.*, 2009, **27**(1), 76–83, DOI: **10.1016/J.BIOTECHADV.2008.09.002**.

25 V. K. Sharma, R. A. Yngard and Y. Lin, Silver nanoparticles: Green synthesis and their antimicrobial activities, *Adv. Colloid Interface Sci.*, 2009, **145**(1–2), 83–96, DOI: **10.1016/J.CIS.2008.09.002**.

26 J. Yin, Y. Yang, Z. Hu and B. Deng, Attachment of silver nanoparticles (AgNPs) onto thin-film composite (TFC) membranes through covalent bonding to reduce membrane biofouling, *J. Membr. Sci.*, 2013, **441**, 73–82, DOI: **10.1016/j.memsci.2013.03.060**.

27 L. Huang, S. Zhao, Z. Wang, J. Wu, J. Wang and S. Wang, In situ immobilization of silver nanoparticles for improving permeability, antifouling and anti-bacterial properties of ultrafiltration membrane, *J. Membr. Sci.*, 2016, **499**, 269–281, DOI: **10.1016/j.memsci.2015.10.055**.

28 Y. Yu, Z. Zhou, G. Huang, H. Cheng, L. Han, S. Zhao, Y. Chen and F. Meng, Purifying water with silver nanoparticles (AgNPs)-incorporated membranes: Recent advancements and critical challenges, *Water Res.*, 2022, **222**, 118901, DOI: **10.1016/J.WATRES.2022.118901**.

29 N. M. Justino, D. S. Vicentini, K. Ranjbari, M. Bellier, D. J. Nogueira, W. G. Matias and F. Perreault, Nanoparticle-templated polyamide membranes for improved biofouling resistance, *Environ. Sci.: Nano*, 2021, **8**(2), 565–579, DOI: **10.1039/d0en01101k**.

30 A. Mocanu, E. Rusen and A. Diacon, *et al.* Antimicrobial properties of polysulfone membranes modified with carbon nanofibers and silver nanoparticles, *Mater. Chem. Phys.*, 2019, **223**, 39–45, DOI: **10.1016/J.MATCHEMPHYS.2018.10.002**.

31 A. C. Mecha, M. N. Chollom, B. F. Babatunde, E. K. Tetteh and S. Rathilal, Versatile Silver-Nanoparticle-Impregnated Membranes for Water Treatment: A Review, *Membranes*, 2023, **13**(4), 432, DOI: **10.3390/MEMBRANES13040432**.

© 2024 The Author(s). Published by the Royal Society of Chemistry

RSC Appl. Interfaces, 2024, **1**, 1186–1197 | **1195**

32 J. Wu, C. Yu and Q. Li, Regenerable antimicrobial activity in polyamide thin film nanocomposite membranes, *J. Membr. Sci.*, 2015, **476**, 119–127, DOI: **10.1016/J.MEMSCI.2014.11.030**.

33 B. Bolto and Z. Xie, Recent Developments in Fouling Minimization of Membranes Modifed with Silver Nanoparticles, *J. Membr. Sci. Res.*, 2018, **4**(3), 111–120, DOI: **10.22079/JMSR.2018.79056.1168**.

34 Z. Yang, Y. Wu, J. Wang, B. Cao and C. Y. Tang, In situ reduction of silver by polydopamine: A novel antimicrobial modification of a thin-film composite polyamide membrane, *Environ. Sci. Technol.*, 2016, **50**(17), 9543–9550, DOI: **10.1021/acs.est.6b01867**.

35 J. Wu, C. Yu and Q. Li, Novel regenerable antimicrobial nanocomposite membranes: Effect of silver loading and valence state, *J. Membr. Sci.*, 2017, **531**, 68–76, DOI: **10.1016/j.memsci.2017.02.047**.

36 A. Soroush, W. Ma, M. Cyr, M. S. Rahaman, B. Asadishad and N. Tufenkji, In Situ Silver Decoration on Graphene Oxide-Treated Thin Film Composite Forward Osmosis Membranes: Biocidal Properties and Regeneration Potential, *Environ. Sci. Technol. Lett.*, 2016, **3**(1), 13–18, DOI: **10.1021/ACS.ESTLETT.5B00304**.

37 P. Xu, C. Cen and N. Chen, *et al.* Facile fabrication of silver nanoparticles deposited cellulose microfiber nanocomposites for catalytic application, *J. Colloid Interface Sci.*, 2018, **526**, 194–200, DOI: **10.1016/j.jcis.2018.04.045**.

38 D. Chen, J. R. Werber, X. Zhao and M. Elimelech, A facile method to quantify the carboxyl group areal density in the active layer of polyamide thin-film composite membranes, *J. Membr. Sci.*, 2017, **534**, 100–108, DOI: **10.1016/j.memsci.2017.04.001**.

39 A. C. Barrios, D. Carrillo, T. R. Waag, D. Rice, Y. Bi, R. Islam and F. Perreault, Prolonging the antibacterial activity of nanosilver-coated membranes through partial sulfidation, *Environ. Sci.: Nano*, 2020, **7**(9), 2607–2617, DOI: **10.1039/d0en00300j**.

40 J. He, T. Kunitake and A. Nakao, Facile In Situ Synthesis of Noble Metal Nanoparticles in Porous Cellulose Fibers, *Chem. Mater.*, 2003, **15**(23), 4401–4406, DOI: **10.1021/cm034720r**.

41 J. Cai, S. Kimura, M. Wada and S. Kuga, Nanoporous cellulose as metal nanoparticles support, *Biomacromolecules*, 2009, **10**(1), 87–94, DOI: **10.1021/bm800919e**.

42 K. C. Song, S. M. Lee, T. S. Park and B. S. Lee, Preparation of colloidal silver nanoparticles by chemical reduction method, *Korean J. Chem. Eng.*, 2009, **26**(1), 153–155, DOI: **10.1007/S11814-009-0024-Y/METRICS**.

43 C. Dong, Z. Wang, J. Wu, Y. Wang, J. Wang and S. Wang, A green strategy to immobilize silver nanoparticles onto reverse osmosis membrane for enhanced anti-biofouling property, *Desalination*, 2017, **401**, 32–41, DOI: **10.1016/j.desal.2016.06.034**.

44 Z. Habib, S. J. Khan, N. M. Ahmad, H. M. A. Shahzad, Y. Jamal and I. Hashmi, Antibacterial behaviour of surface modified composite polyamide nanofiltration (NF) membrane by immobilizing Ag-doped TiO2 nanoparticles, *Environ. Technol.*, 2020, **41**(28), 3657–3669, DOI: **10.1080/09593330.2019.1617355**.

45 T. A. Dankovich and D. G. Gray, Bactericidal paper impregnated with silver nanoparticles for point-of-use water treatment, *Environ. Sci. Technol.*, 2011, **45**(5), 1992–1998, DOI: **10.1021/es103302t**.

46 G. Goncalves, P. A. A. P. Marques, C. M. Granadeiro, H. I. S. Nogueira, M. K. Singh and J. Grácio, Surface modification of graphene nanosheets with gold nanoparticles: The role of oxygen moieties at graphene surface on gold nucleation and growth, *Chem. Mater.*, 2009, **21**(20), 4796–4802, DOI: **10.1021/cm901052s**.

47 T. J. Zimudzi, K. E. Feldman, J. F. Sturnfield, A. Roy, M. A. Hickner and C. M. Stafford, Quantifying Carboxylic Acid Concentration in Model Polyamide Desalination Membranes via Fourier Transform Infrared Spectroscopy, *Macromolecules*, 2018, **51**(17), 6623–6629, DOI: **10.1021/acs.macromol.8b01194**.

48 C. Y. Tang, Y. N. Kwon and J. O. Leckie, Probing the nano- and micro-scales of reverse osmosis membranes-A comprehensive characterization of physiochemical properties of uncoated and coated membranes by XPS, TEM, ATR-FTIR, and streaming potential measurements, *J. Membr. Sci.*, 2007, **287**(1), 146–156, DOI: **10.1016/j.memsci.2006.10.038**.

49 R. R. Mohamed and M. W. Sabaa, Synthesis and characterization of antimicrobial crosslinked carboxymethyl chitosan nanoparticles loaded with silver, *Int. J. Biol. Macromol.*, 2014, **69**, 95–99, DOI: **10.1016/j.ijbiomac.2014.05.025**.

50 S. Mondal and S. R. Wickramasinghe, Produced water treatment by nanofiltration and reverse osmosis membranes, *J. Membr. Sci.*, 2008, **322**(1), 162–170, DOI: **10.1016/j.memsci.2008.05.039**.

51 Y. N. Kwon and J. O. Leckie, Hypochlorite degradation of crosslinked polyamide membranes. II. Changes in hydrogen bonding behavior and performance, *J. Membr. Sci.*, 2006, **282**(1–2), 456–464, DOI: **10.1016/j.memsci.2006.06.004**.

52 E. Idil Mouhoumed, A. Szymczyk, A. Schäfer, L. Paugam and Y. H. La, Physico-chemical characterization of polyamide NF/RO membranes: Insight from streaming current measurements, *J. Membr. Sci.*, 2014, **461**, 130–138, DOI: **10.1016/j.memsci.2014.03.025**.

53 V. T. Do, C. Y. Tang, M. Reinhard and J. O. Leckie, Degradation of polyamide nanofiltration and reverse osmosis membranes by hypochlorite, *Environ. Sci. Technol.*, 2012, **46**(2), 852–859, DOI: **10.1021/es203090y**.

54 O. Coronell, B. J. Mariñas and D. G. Cahill, Depth heterogeneity of fully aromatic polyamide active layers in reverse osmosis and nanofiltration membranes, *Environ. Sci. Technol.*, 2011, **45**(10), 4513–4520, DOI: **10.1021/ES200007H**.

55 C. L. Ritt, J. R. Werber, M. Wang and M. Elimelech, Ionization behavior of nanoporous polyamide membranes, *Proc. Natl. Acad. Sci. U. S. A.*, 2020, **117**(48), 30191–30200, DOI: **10.1073/PNAS.2008421117/-/DCSUPPLEMENTAL**.

56 E. S. Kim, G. Hwang, M. Gamal El-Din and Y. Liu, Development of nanosilver and multi-walled carbon

nanotubes thin-film nanocomposite membrane for enhanced water treatment, *J. Membr. Sci.*, 2012, **394–395**, 37–48, DOI: **10.1016/j.memsci.2011.11.041**.

57 Y. Yin, T. Li, K. Zuo, X. Liu, S. Lin, Y. Yao and T. Tong, *et al.* Which Surface Is More Scaling Resistant? A Closer Look at Nucleation Theories for Heterogeneous Gypsum Nucleation in Aqueous Solutions, *Environ. Sci. Technol.*, 2022, **56**(22), 16315–16324, DOI: **10.1021/acs.est.2c06560**.

58 S. Y. Lee, H. J. Kim, R. Patel, S. J. Im, J. H. Kim and B. R. Min, Silver nanoparticles immobilized on thin film composite polyamide membrane: Characterization, nanofiltration, antifouling properties, *Polym. Adv. Technol.*, 2007, **18**(7), 562–568, DOI: **10.1002/pat.918**.

59 K. A. Marill and R. J. Lewis, Advanced Statistics: Linear Regression, Part II: Multiple Linear Regression, *Acad. Emerg. Med.*, 2004, **11**(1), 94–102, DOI: **10.1197/J. AEM.2003.09.006**.

60 K. Ranjbari, W. L. Lee, A. Ansari, A. C. Barrios, F. Sharif, R. Islam and F. Perreault, Controlling silver release from antibacterial surface coatings on stainless steel for biofouling control, *Colloids Surf., B*, 2022, **216**, 112562, DOI: **10.1016/J.COLSURFB.2022.112562**.

61 C. Liu, A. F. Faria, J. Jackson, Q. He and J. Ma, Enhancing the anti-fouling and fouling removal properties of thin-film composite membranes through an intercalated functionalization method, *Environ. Sci.: Water Res. Technol.*, 2021, **7**(7), 1336–1347, DOI: **10.1039/D1EW00188D**.

62 M. G. M. de Souza, J. P. Batista and E. H. de Faria, *et al.* Silver nanoparticle incorporation into flexible polyamide 12 membranes, *J. Sol-Gel Sci. Technol.*, 2022, **102**(1), 219–228, DOI: **10.1007/S10971-021-05693-W/FIGURES/10**.

63 A. Syafiuddin, Toward a comprehensive understanding of textiles functionalized with silver nanoparticles, *J. Chin. Chem. Soc.*, 2019, **66**(8), 793–814, DOI: **10.1002/JCCS.201800474**.

© 2024 The Author(s). Published by the Royal Society of Chemistry

RSC Appl. Interfaces, 2024, **1**, 1186–1197 | **1197**